Operating a quantum pump in a closed circuit

2006 J. Phys. A: Math. Gen. 39 3575

(http://iopscience.iop.org/0305-4470/39/14/006)

INSTITUTE OF PHYSICS PUBLISHING JOURNAL OF PHYSICS A: MATHEMATICAL AND GENERAL

J. Phys. A: Math. Gen. **39** (2006) 3575–3592 doi:10.1088/0305-4470/39/14/006

Operating a quantum pump in a closed circuit

Itamar Sela and Doron Cohen

Department of Physics, Ben-Gurion University, Beer-Sheva 84005, Israel

Received 21 December 2005, in final form 6 February 2006
Published 22 March 2006
Online at stacks.iop.org/JPhysA/39/3575

Abstract

During an adiabatic pumping cycle a conventional two-barrier quantum device takes an electron from the left lead and ejects it to the right lead. Hence, the pumped charge per cycle is naively expected to be $Q \leqslant e$. This zero-order adiabatic point of view is in fact misleading. For a closed device we can get $Q > e$ and even $Q \gg e$. In this paper, a detailed analysis of the quantum pump operation is presented. Using the Kubo formula for the geometric conductance, and applying the Dirac chains picture, we derive practical estimates for Q.

PACS numbers: 03.65.−w, 03.65.Vf, 73.23.−b, 05.45.Mt

(Some figures in this article are in colour only in the electronic version)

1. Introduction

Understanding of charge transport in mesoscopic and molecular size devices is essential for the future realization of 'quantum circuits' [1]. Of particular interest are adiabatic processes that take electrons and move them one by one via a device. The simple-minded peristaltic point of view of such process is misleading: such picture looks valid in the case of an open circuit, but breaks down once the pump is integrated into a closed circuit [2–4]. It is the purpose of this paper to further elaborate on the physics of quantum pumping in *closed circuits* and to provide a detailed analysis of a prototype pump. The interest and the feasibility of realizing experiments with closed circuits is discussed in section 1.3 of [5].

1.1. The prototype pumping device

The prototype example for a quantum pumping device is the two-barrier model (figure 1). The one particle Hamiltonian is

$$\mathcal{H}(X_1(t), X_2(t)) = \frac{1}{2\mathsf{m}}\hat{p}^2 + X_1(t)\delta(\hat{x} - x_1) + X_2(t)\delta(\hat{x} - x_2) \tag{1}$$

where m is the mass of the particle and $(\hat{x}, \hat{p})$ are the position and the momentum operators. The region $x < x_1$ is the left lead and the region $x > x_2$ is the right lead. We refer to the segment $x_1 < x < x_2$ as the 'dot region'. The driving is performed by changing X_1 and X_2 in time. In an actual experiment, the control parameters X_1 and X_2 represent gate voltages.

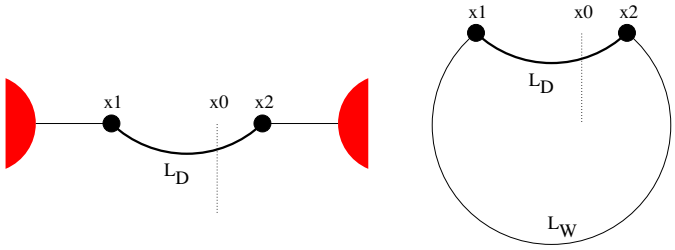

Figure 1. Illustration of the model system. The two-barrier pumping device is used in two different configurations. Left panel: open lead geometry; right panel: closed ring geometry. The barriers are located at the nodes x_1 and x_2 while the current is measured through the section at x_0.

In order to talk about charge transfer we have to also define a current operator. In what follows, we use the conventional definition

$$\mathcal{I} = \frac{e}{2\mathsf{m}}(\hat{p}\delta(\hat{x} - x_0) + \delta(\hat{x} - x_0)\hat{p}) \tag{2}$$

where e is the charge of the particle and x_0 is an arbitrary section point. The momentary current via different sections is in general not the same. But if we integrate it over a whole pumping cycle the result becomes independent of x_0.

The pumping device can be used in two different configurations. In the case of an *open geometry* (figure 1), the leads are attached to reservoirs that have the same chemical potentials. For simplicity, one assumes a zero-temperature Fermi occupation.

In the case of a *closed geometry* (figure 1), the leads are detached from the reservoirs and are connected together so as to have a ring. This means periodic boundary conditions over a large space interval $(-L/2) < x < (L/2)$. Furthermore, the closed system is assumed to be strictly isolated from any environmental influences. The closed system can be regarded as a network with two nodes that are connected by two bonds one of length L_{D} (dot region) and the other of length L_{W} (wire region). The total length of the ring is $L = L_{\mathrm{D}} + L_{\mathrm{W}}$. We assume that $L_{\mathrm{D}} \ll L$.

1.2. Open (leads) geometry

The *open version* of the two barrier model has been considered in [6] using the scattering matrix formalism of Büttiker Prétre and Thomas (BPT) [7, 8]. A typical pumping cycle is illustrated in figure 2(*c*). In the first half of the cycle an electron is taken from the left lead into the dot region via the left barrier, while in the second half of the cycle an electron is transferred from the dot region to the right lead via the right barrier. Naively, by this peristaltic picture, it seems that at most one electron is pumped through the device per cycle. This expectation is supported by the formal calculation. Using the BPT formula one obtains [9]

$$Q = (1 - \overline{g}_{\mathrm{T}})e \tag{3}$$

where $0 < \overline{g}_{\mathrm{T}} < 1$ characterizes the transmission of the device during the charge transfer. In the limit $\overline{g}_{\mathrm{T}} \to 0$, which is a pump with *no leakage*, indeed one gets $Q = e$. Otherwise one gets $Q < e$.

1.3. Closed (ring) geometry

Our interest is in the *closed version* of the two barrier model. A major observation is that the pumped charge Q is *not* 'quantized' even if the device is closed and isolated from any

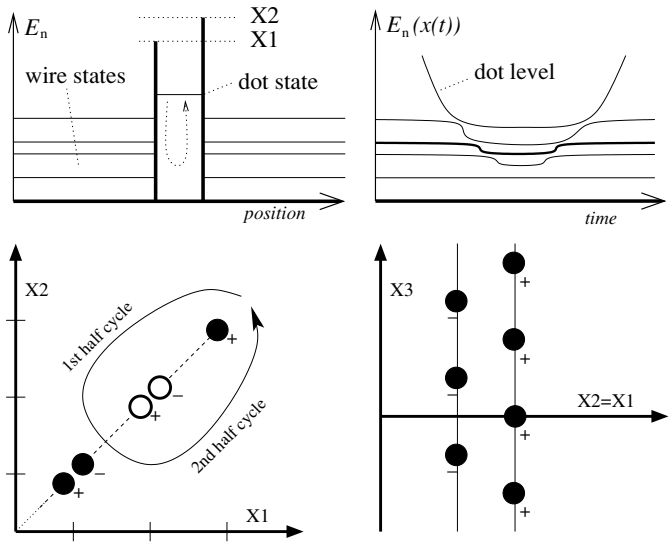

Figure 2. (*a*) Upper left: the energy levels of a ring with two barriers, at the beginning of the pumping cycle. It is assumed that the three lower levels are occupied. (*b*) Upper right: the adiabatic levels as a function of time during the pumping cycle. (*c*) Lower left: the (X_1, X_2) locations of the Dirac chains of the three occupied levels. Filled (hollow) circles imply that there is (no) monopole in the pumping plane. Note that for the sake of illustration overlapping chains are displaced from each other. The pumping cycle encircles $2 + 1$ Dirac chains that are associated with the third and second levels, respectively. (*d*) Lower right: the two Dirac chains that are associated with the third level.

environmental influences. Moreover, it can be larger than unit charge. In fact, we can have $Q \gg e$.

The analysis that we are going to present demonstrates and refines general results that were obtained in [3]. There we have worked out an artificial circuit which has been modelled as a three-site system. In the present paper, we would like to work out a major prototype model that allows the desired comparison between results for closed circuit as opposed to that of open geometry equation (3).

We are going to use the Kubo approach to quantum pumping [2–4]. The 'Dirac chains picture' which we further review in the next subsection makes a distinction between 'near-field' and 'far-field' pumping cycles. The near-field result has been further considered in [10] using an extension of the BPT scattering approach to quantum pumping.

1.4. The Dirac chains picture

In order to analyse an *adiabatic* [11] pumping cycle, we have first to understand the geometry of the parameter space. In fact, the parameter space of the two-barrier model is three dimensional (X_1, X_2, X_3) where $X_3 = \Phi$ is the flux via the ring. In practice, we assume a planar $\Phi = 0$ pumping cycle, but for the theoretical discussion it is convenient to regard Φ as a free parameter.

We ask what is the amount of charge which is transported via a section of the ring per cycle. For this purpose, we have to calculate the current $I = \langle \mathcal{I} \rangle$ at each moment. If we were changing the flux we would have by Ohm law $I = -G^{33}\dot{\Phi}$ where G^{33} is called the Ohmic (dissipative) conductance. But if we change (say) the parameter X_1 then $I = -G^{31}\dot{X}_1$, where G^{31} is called the geometric (non-dissipative) conductance [12–14]. In general we can write $\mathrm{d}Q = -G^{31}\mathrm{d}X_1 - G^{32}\mathrm{d}X_2$ and hence

$$Q = \oint I\,\mathrm{d}t = \oint \boldsymbol{G}\cdot\mathrm{d}\boldsymbol{X} \tag{4}$$

where $\boldsymbol{X} = (X_1, X_2)$ and $\boldsymbol{G} = (G^{31}, G^{32})$.

The elements of the conductance matrix G^{kj} can be calculated using the Kubo formula. It turns out [11, 14] that in the adiabatic limit $G^{31} = B_2$ and $G^{32} = -B_1$ where $\vec{B}$ is the 'magnetic' field (2-form) which appears in the theory of Berry phase [11]. The sources of this field are Dirac monopoles that are located at the points of degeneracy. For the double barrier model, a given level n can have a degeneracy provided $X_1 = X_2$ and either $\Phi = 0$ or $\Phi = \pi\hbar/e$ modulo $2\pi\hbar/e$. In fact, we have for each level (excluding the ground state) two Dirac chains of degeneracies as in figure 2(*d*).

From the above observation, one easily draws the following conclusions: (i) we can get $Q \gg e$ for a tight cycle around a Dirac chain if the degeneracy is in the pumping plane. (ii) We can get $Q \ll e$ for a tight cycle around a Dirac chain if the degeneracy is off the pumping plane. (iii) We can get $Q \sim e$ for a cycle which is located in the far field of a Dirac chain. The existence of a far-field region is not self-evident. This constitutes a major motivation for the present study.

1.5. Outline

The outline of this paper is as follows. In section 2, we clarify the starting point of the calculation, which is the Kubo formula. In section 3, we introduce a preliminary discussion of the expected results and their significance. Then, in sections 4–11 we analyse the pumping process in the two-barrier model. In particular, we find the dependence of Q on the 'radius' of the pumping cycle and make a distinction between 'near-field' and 'far-field' results.

2. The Kubo formula

Given a time-dependent Hamiltonian $\mathcal{H}(X)$ with $X = X(t)$, we define $\mathcal{F} = -\partial\mathcal{H}/\partial X$ and would like to calculate the generalized conductance as defined by the expression

$$\langle\mathcal{I}\rangle = -G\dot{X}. \tag{5}$$

We label by n the adiabatic levels of the closed ring. The adiabatic states are defined by the equation $\mathcal{H}|n\rangle = E_n|n\rangle$ with implicit X dependence. Using these notation the Kubo formula for the *geometric conductance* can be written as

$$G = \sum_{m(\neq n)} \frac{2\hbar\mathcal{F}_{mn}}{(E_m - E_n)^2}\,\mathrm{Im}[\mathcal{I}_{nm}]. \tag{6}$$

The above expression assumes that only one level (n) is occupied. If several levels are occupied we have to sum over them. If we have more than one control variable, say X_1 and X_2, then we have to use the more elaborated notation G^{31} and G^{32} in order to distinguish between different elements of the conductance matrix.

If the pumping cycle crosses very close to a degeneracy, we can get from equations (5)–(6) a very large current I, and upon integration we can find that the transported charge is $Q \gg e$. In the next sections, we shall develop actual estimates for Q. But first we would like to further illuminate the significance of Q.

The Schrödinger equation can be written in the *adiabatic basis*, where the *transformed* Hamiltonian matrix takes the form $H_{nm} = E_n\delta_{nm} + \dot{X}A_{nm}$, where E_n are called the adiabatic energy levels and A_{nm} is a matrix that can be calculated using a well-known recipe (which is summarized in section 3 of [3]). One regards $\dot{X}$ as the 'small parameter'. If the system

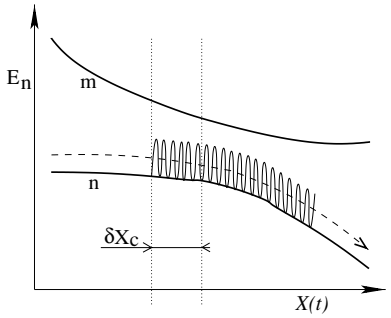

Figure 3. Cartoon of the adiabatic evolution within the framework of the two-level approximation. The system is prepared in level n, and the nearby empty level is $m = n + 1$. The control parameter $X(t)$ is being changed slowly and therefore the system 'oscillates' around the first-order adiabatic solution. The energy of the latter is illustrated by a dashed line. Note that the identity of the adiabatic state changes gradually and can be regarded as constant only on scales $\delta X \ll \delta X_c$.

is prepared in an instantaneous *adiabatic* state $|n\rangle$, then the instantaneous current is $I = 0$, whereas if it is prepared in an instantaneous *steady* state (an eigenstate of H_{nm}), then the instantaneous current is finite, say $I = I_0$. Accordingly one can question the physical relevance of Q: after all typically the initial preparation is an adiabatic state and not a steady state.

So let us consider an actual physical scenario. For simplicity, we assume that only two adiabatic levels are involved: the occupied level n and next (empty) level $m = n + 1$. To make the dynamical picture simple, we use an analogy with the dynamics of a spin $1/2$ particle and consider the illustration in figure 3. We regard the state n as spin polarized in the z direction and the state m as spin polarized in the $-z$ direction. The instantaneous steady states of the Hamiltonian are polarized along an axis that has a small tilt relative to the z direction.

Initially, the spin is polarized in the z direction and therefore $I(t = 0) = 0$. For some time we have $|X(t) - X(0)| \ll \delta X_c$ where δX_c is the relevant parametric scale for the variation of the adiabatic levels. During this time interval the tilt angle is approximately constant. The spin is performing a precession around the tilted axis. As a result, we get $I(t) \neq 0$. In fact, the maximum current is $I(t) = 2I_0$. We get this current after half period of precession.

So, we have a modulated current $I(t)$ that equals upon averaging I_0. As long as $|X(t) - X(0)| \ll \delta X_c$, the precession goes on as described above. But on larger time scales we have to take into account the variation in the tilt angle. Consequently, the modulation of the current is no longer in the range $0 < I(t) < 2I_0$, but rather it is shifted and may increase. Still the average stays approximately I_0.

Thus, we see that in the actual physical scenario the average over $I(t)$ is the same as the I_0 of the instantaneous steady state. The validity conditions for this statement are essentially the validity conditions of linear response theory, which are further explained in [3]. The above discussion illuminates the justification for the use of the first-order steady-state solution of Kubo for the purpose of evaluating the pumped charge in an actual physical scenario.

3. Charge transfer during an avoided crossing

The pumped charge Q is obtained via the integral equation (4) using equation (6) for G. On the basis of the naive heuristic picture of the introduction (and see figure 2), we expect that most of the contribution to the integral would come from a small segments in $\boldsymbol{X}$ space where the

last occupied level has an avoided crossing with the first unoccupied level. Later we precisely define the region in $\boldsymbol{X}$ space where this assumption is a valid approximation.

Let us try to sketch what might come out from the calculation. Later on we are going to do a proper job. But before we dive into the detailed analysis (which is quite lengthy), it would be nice to gain some rough expectation. Given that our interest is focused in a small energy window such that $E_n \sim E$, we define $v_{\rm E} = (2E/\mathsf{m})^{1/2}$. The mean level spacing in the energy range of interest is

$$\Delta = v_{\rm E}\frac{\hbar\pi}{L} \tag{7}$$

while the energy splitting Δ_s at the avoided crossing might be much smaller. We define the following notation:

$$|\mathcal{F}_{nm}| \equiv \sigma_0 \tag{8}$$

$$|\mathcal{I}_{nm}| \equiv \frac{ev_{\rm E}}{L}\sqrt{g_\varphi} \tag{9}$$

$$\Delta_s/\Delta \equiv \sqrt{1-g_0} \tag{10}$$

where both $0 < g_\varphi < 1$ and $0 < g_0 < 1$ are dimensionless. Note that g_0 is related to the overall transmission $\overline{g}_{\rm T}$ of the device. The adiabaticity condition is

$$|\dot{X}| \ll \frac{\Delta_s^2}{\hbar\sigma_0} \tag{11}$$

and from equation (5) with (6) we get the current

$$\langle\mathcal{I}\rangle = 2\left(\frac{\hbar\sigma_0}{\Delta_s^2}\dot{X}\right)\left(\frac{ev_{\rm E}}{L}\right)\sqrt{g_\varphi}. \tag{12}$$

The time of the Landau–Zener transition via the avoided crossing is

$$\delta t \approx (\Delta_0/\sigma_0)/\dot{X} \tag{13}$$

and hence the transported charge is

$$Q \approx \langle\mathcal{I}\rangle\delta t \approx \left(\frac{g_\varphi}{1-g_0}\right)^{1/2} e \tag{14}$$

where g_0 and g_φ should be estimated in the region of the avoided crossing. We note that $g_\varphi/(1-g_0)$ is like the Thouless conductance and can be regarded as a measure for the sensitivity of the energy levels to a test flux. We have pointed out and discussed this issue in [2, 3], and later it was derived [10] in the context of the scattering formalism.

In figure 4, we display the numerically determined Q for various path segments. The horizontal axis is the $|X_1 - X_2|$ distance of the path segment from the degeneracy point. As $|X_1 - X_2|$ becomes small $g_0 \to 1$ and we get $Q \gg e$. But the asymptotic value $Q \approx e$ which is observed for large $|X_1 - X_2|$ cannot be explained by such a simple-minded calculation. A major objective of the detailed analysis is to illuminate the observed crossover.

4. The model, basic equations

The one particle Hamiltonian of the two-barrier model depends on the set of parameters (X_1, X_2, Φ). From now on we use units such that $e = \hbar = 1$ and characterize the geometry by the dimensionless parameter

$$b = L_{\rm W}/L_{\rm D} \gg 1 \tag{15}$$

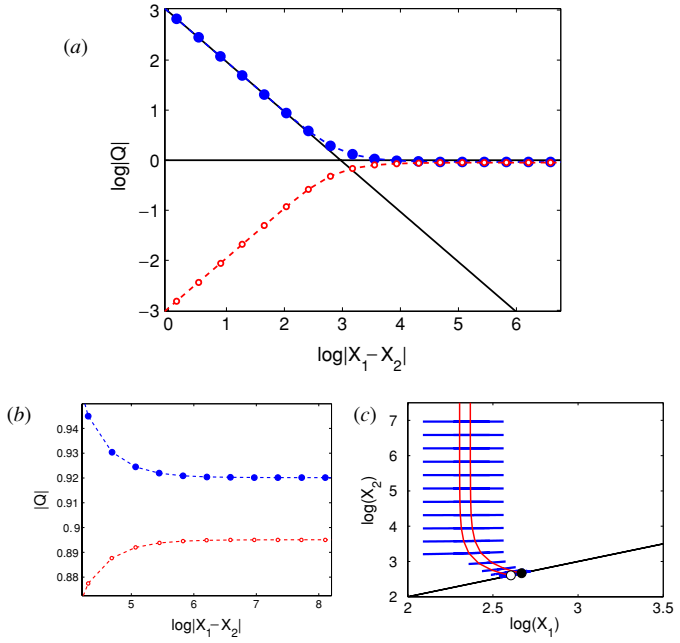

Figure 4. Panels (*a*) and (*b*): numerical calculation of the pumped charge Q. The model parameters are $L_{\rm D} = \mathsf{m} = e = 1$ and $L_{\rm W} = 3000.43$. The current I is measured at the middle of the dot. The numerical integration is carried out along the segments which are indicated in panel (*c*) and the results are multiplied by 2 so as to include the equal contribution that comes from the second half of the cycle. There are two sets of data points. One set (filled circles) is for pumping cycles that encircle an in-plane degeneracy point ($n_r = 2993$). A second set (hollow circles) is for pumping cycles that encircle an off-plane degeneracy point ($n_r = 2992$). The location of the avoided crossing for each data set is indicated by the solid lines in panel (*c*). The near- and the far-field approximations that we derive for Q are indicated by the solid lines in panel (*a*). The zoom in panel (*b*) reveals that Q in the far field is in fact slightly less than 1, which is explained in section 13.

We write the wavefunction on the two bonds as

$$\psi_{\rm dot}(x) = (2/L)^{1/2}\sqrt{q_{\rm D}}\sin(\varphi_{\rm D}(x)) \tag{16}$$

$$\psi_{\rm wire}(x) = (2/L)^{1/2}\sqrt{q_{\rm W}}\sin(\varphi_{\rm W}(x)) \tag{17}$$

where $\varphi(x) = kx + \text{const}$. Given (X_1, X_2) and assuming $\Phi = 0$, the eigenstates of this Hamiltonian can be found by searching k_n values for which the matching conditions on the log-derivatives are satisfied. This leads to the following system of equations:

$$\cot(\varphi_{\rm W1}) + \cot(\varphi_{\rm D1}) = \frac{2\mathsf{m}}{k}X_1 \tag{18}$$

$$\cot(\varphi_{\rm W2}) + \cot(\varphi_{\rm D2}) = \frac{2\mathsf{m}}{k}X_2 \tag{19}$$

$$\varphi_{\rm D2} - \varphi_{\rm D1} = kL_{\rm D} \tag{20}$$

$$\varphi_{\rm W2} - \varphi_{\rm W1} = kL_{\rm W} \tag{21}$$

where it should be clear that $\varphi_{\rm D1} \equiv \varphi_{\rm D}(x_1)$, etc. The corresponding eigenenergies are $E_n = k_n^2/2\mathsf{m}$. A similar system of equations can be written for $\Phi = \pi$. We can find the $q_{\rm W}/q_{\rm D}$ ratio for a given eigenstate via the matching condition on the wavefunction at either of the

two nodes:

$$\sqrt{q_{\mathrm{W}}}\sin(\varphi_{\mathrm{W}}) = \sqrt{q_{\mathrm{D}}}\sin(\varphi_{\mathrm{D}}) \tag{22}$$

where $(\varphi_{\mathrm{D}}, \varphi_{\mathrm{W}})$ mean either $(\varphi_{\mathrm{D1}}, \varphi_{\mathrm{W1}})$ or $(\varphi_{\mathrm{D2}}, \varphi_{\mathrm{W2}})$. The normalization condition implies that

$$\frac{L_{\mathrm{D}}}{L}q_{\mathrm{D}} + \frac{L_{\mathrm{W}}}{L}q_{\mathrm{W}} \approx 1. \tag{23}$$

For an 'ergodic state' we have $q \approx 1$ for both bonds. In general, we characterize an eigenstate by the mixing parameter

$$\Theta \equiv 2\arctan\left(\sqrt{\frac{\mathrm{Prob(wire)}}{\mathrm{Prob(dot)}}}\right) = 2\arctan\left(\sqrt{b}\left(\frac{q_{\mathrm{W}}}{q_{\mathrm{D}}}\right)^{1/2}\right) \tag{24}$$

such that $\Theta = 0$ means a definite dot state, while $\Theta = \pi$ means a definite wire state. In practice, we have $0 < \Theta < \pi$.

In the numerical analysis, we use units such that $\mathsf{m} = 1$ and $L_{\mathrm{D}} = 1$. Given X_1 and X_2, we solve the system of equations for k_n and for $\varphi^{(n)}$ at the nodes. Then we determine $q^{(n)}$ at each bond, and from the ratio we get $\Theta^{(n)}$ as well.

5. Regions in X space

We focus on a small energy window such that the energy levels of interest are $E < E_n < E + \mathrm{d}E$. We characterize a barrier $X\delta()$ using its transmission

$$g(X) = \left[1 + \left(\frac{1}{v_{\mathrm{E}}}X\right)^2\right]^{-1} \approx \left(\frac{1}{v_{\mathrm{E}}}X\right)^{-2}. \tag{25}$$

The last expression holds if $g(X) \ll 1$. We can regard $g_1 = g(X_1)$ and $g_2 = g(X_2)$ as an alternate way to specify X_1 and X_2. The (X_1, X_2, Φ) space is divided into various regions (figure 5(*a*)). There is a region where g_1 and g_2 are of order 1 ($|1 - g| \ll 1$). There the delta functions at the nodes can be treated as a small perturbation. There is a region where $1/b \ll g_1, g_2 \ll 1$. There each dot level mixes with many wire levels. This intermediate region will be discussed in a future work [15]. Finally, there is the region in $\boldsymbol{X}$ space which is of interest in the present study:

$$g_1, g_2 \ll 1/b. \tag{26}$$

We shall argue that in this region the states are categorized into 'wire states' and 'dot state', which mix only whenever the energy level of the dot 'cross' an energy level of the wire (figures 5(*b*)–(*d*)). This allows to use 'two-level' approximation in the analysis of the mixing.

The degeneracies of the Hamiltonian occur at points $(X^{(r)}, X^{(r)})$ along the symmetry axis of $\boldsymbol{X}$ space. They are divided into two groups: those that are located in the $\Phi = 0(\mathrm{mod}(2\pi))$ planes and those that are located in the $\Phi = \pi(\mathrm{mod}(2\pi))$ planes. In the appendix, we find the explicit expression for $X^{(r)}$. It should be clear that each degeneracy point is duplicated $\mathrm{mod}(2\pi)$ in the Φ direction, hence creating what we call a 'Dirac chain'.

There are only two non-trivial degeneracies in $\boldsymbol{X}$ space which are associated with a given level n. One is with the neighbouring level 'from above' and the other is with the neighbouring level 'from below'.

Once we locate a degeneracy point, we can make a distinction between 'near-field' and 'far-field' regions. The near field is defined as the region where we can use degenerate perturbation theory in order to figure out the splitting of the levels. In contrast to that, the far

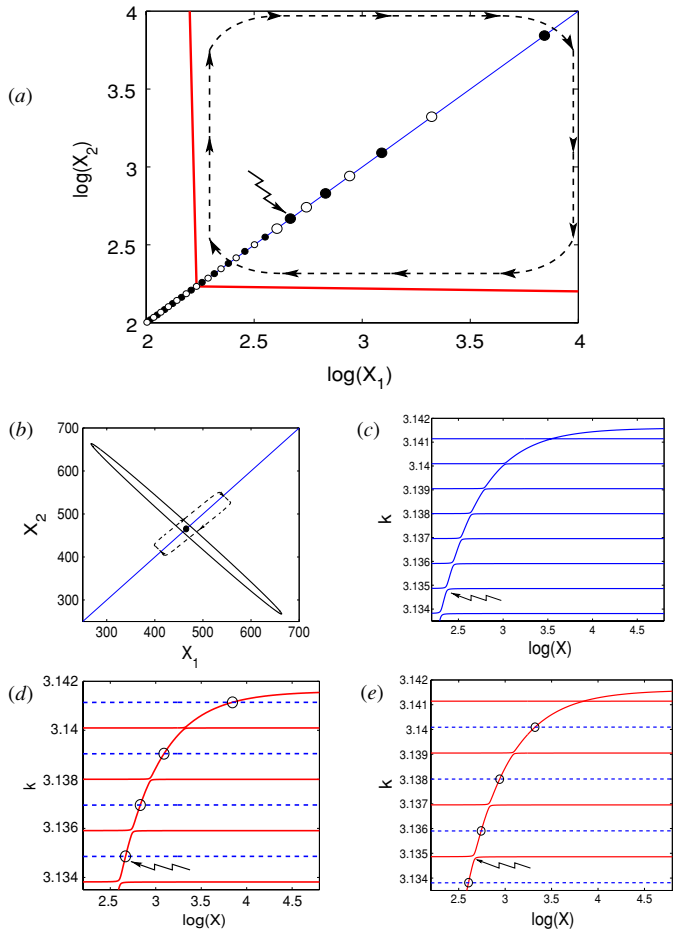

Figure 5. Regions in $\boldsymbol{X}$ space. The model parameters are the same as in the previous figure. Panel (a) displays the region of interest as defined in equation (26). It is bounded by the left and by the bottom solid lines which are defined by $g(X) \sim 1/b$. In-plane and off-plane degeneracy points are indicated by filled and hollow circles, respectively. We indicate by arrow one in-plane degeneracy point ($n_r = 2993$). A zoom of its near field is displayed in panel (b). The ellipse in panel (b) indicates a level splitting that equals $\Delta/10$. The dashed lines in panels (a) and (b) indicate far-field and near-field pumping cycles, respectively. In panels (c)–(e) we show the energy levels (k_n) along three paths in $\vec{X}$ space, which are ($X_1 = X, X_2 = \infty, \Phi = 0$), ($X_1 = X, X_2 = X, \Phi = 0$) and ($X_1 = X, X_2 = X, \Phi = \pi$), respectively. The degeneracies $n_r = 2992 \ldots 2999$ are circled. The arrow indicates the representative degeneracy point $n_r = 2993$. In panels (d), the odd states are indicated by dashed lines so as to distinguish them from the even states.

field is defined as the region where we can calculate the splitting of the levels by treating the dot–wire coupling as a first-order perturbation.

In figure 5(a), we show one pumping path that crosses in the near-field region and a second pumping path that crosses in the far-field region.

6. Eigenstate analysis

In the theoretical analysis, it is illuminating to map the behaviour of k_n and $\Theta^{(n)}$ in (X_1, X_2, Φ) space. See figures 6 and 7. It is not difficult to realize that the variation of Θ is bounded as

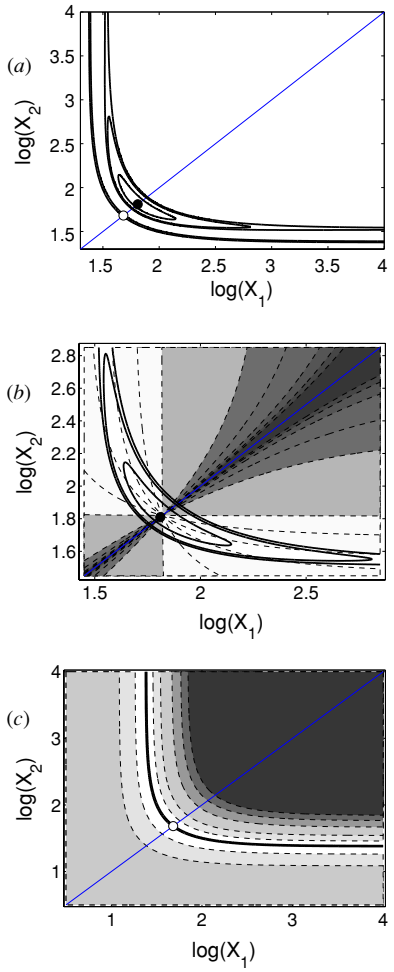

Figure 6. The energy level splitting and the mixing parameter Θ for two pairs of levels. The model parameters are $L_{\mathrm{D}} = \mathsf{m} = e = 1$ and $L_{\mathrm{W}} = 160.43$. In panel (*a*), we show the contour lines for the energy level splitting of the first (even) dot level with an odd wire level ($n = 158$) and for the energy level splitting of the first (even) dot level with an even wire level ($n = 157$). The two cases are displayed again in panels (*b*) and (*c*), respectively, where we plot both level splitting contours (solid lines) and Θ contours (dashed lines). In the 'even–odd crossing' case we have an in-plane degeneracy, which is indicated by a filled circle, while the inner most contour line is for $\Delta/5$ splitting. Note that within the white regions the mixing is maximal ($\Theta \sim \pi/2$). In the 'even–even avoided crossing' case the projection of the off-plane degeneracy point is indicated by a hollow circle.

follows:

$$\sqrt{b}\left[\frac{1}{4}g\right]^{+1/2} < \tan(\Theta/2) < \sqrt{b}\left[\frac{1}{4}g\right]^{-1/2} \tag{27}$$

where g is either g_1 or g_2. The derivation of this result is as follows: the matching conditions at a given node implies that $(\varphi_{\mathrm{D}}, \varphi_{\mathrm{W}})$ are constraint to be on one of two branches which are illustrated in figure 8. With each point of a given branch, we can associate a Θ value via equation (24) and either equation (18) or equation (19). It is a straightforward exercise

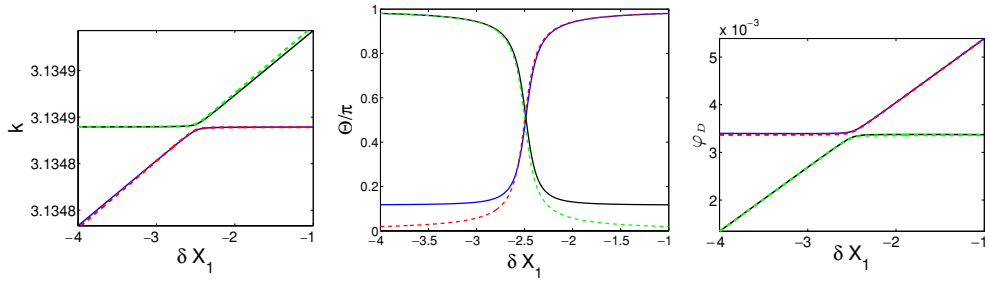

Figure 7. Tests of the perturbation theory based approximations (dashed lines) against the numerics (solid lines). The model parameters are $L_{\rm D} = \mathsf{m} = e = 1$ and $L_{\rm W} = 3000.43$, and we focus on the degeneracy point $n_r = 2993$. For these parameters, $X^{(r)} \approx 465$ and $g^{(r)} \approx 4.5 \times 10^{-5}$. All the plots refer to the path $(X_2 - X_1) = 5$. In the left panel, the dashed lines are derived from equation (37). In the middle panel, the dashed lines are based on equations (40) and (41) with θ from equation (36). In the right panel, the dashed lines are deduced from equation (30).

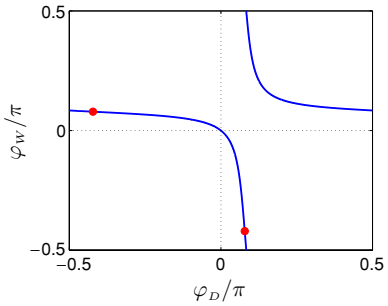

Figure 8. The wire phase $\varphi_{\rm W}/\pi$ versus the dot phase $\varphi_{\rm D}/\pi$ at a node with delta barrier $g(X) = 0.225$. The two branches are implied by the matching condition (18). The ratio $|\sin(\varphi_{\rm D})/\sin(\varphi_{\rm D})|$ attains its extremal values (equation (27)) at the points which are indicated by circles.

to express Θ, say, as a function of $\varphi_{\rm D}$ and then to find its minimum and maximum values. Assuming that $g \ll 1$ one obtains equation (27).

Given $\Theta^{(n)}$ we can extract what are $q^{(n)}$ at each bond and what are $\varphi^{(n)}$ at the nodes. By solving equation (23) with equation (24) we get

$$q_{\rm D} = b(\cos(\Theta/2))^2 \tag{28}$$

$$q_{\rm W} = (\sin(\Theta/2))^2 \tag{29}$$

then from equation (22) with either equation (18) or equation (19) we find an expression for φ at a given node. In particular, we get

$$\varphi_{\rm D} = \left(1 \pm \frac{1}{\sqrt{b}} \tan(\Theta/2) + \cdots\right) \left[\frac{1}{4} g\right]^{1/2}. \tag{30}$$

Note that φ is well-defined mod(π). There are states which are dot like ($\Theta \ll 1$) and there are states which are wire like ($\Theta \sim \pi$). There are regions where a dot-like state mixes with wire-like state leading to pair of states with $\Theta^{(+)} \sim \Theta^{(-)} \sim \pi/2$. From the above formula, it follows that in the latter case

$$\varphi_{\rm D}^{(+)} \approx \varphi_{\rm D}^{(-)} \approx \left[\frac{1}{4} g\right]^{1/2} \tag{31}$$

$$|\varphi_{\rm D}^{(+)} - \varphi_{\rm D}^{(-)}| = \frac{1}{\sqrt{b}}\left[\frac{1}{4}g\right]^{1/2}\left(\tan(\Theta^{(+)}/2) + \tan(\Theta^{(-)}/2)\right). \tag{32}$$

7. Eigenenergies and 'mixing' from perturbation theory

In order to find the splitting and the mixing of the two levels, we use perturbation theory once in the far-field analysis and once in the near-field analysis. In both cases, we use the following notation. The unperturbed basis is $|i\rangle$ with a dot-like state $|1\rangle$ and a wire-like $|2\rangle$. The perturbed eigenstates $|n\rangle$ are indicated as $|+\rangle$ and $|-\rangle$. The Hamiltonian in both cases has the general form

$$\mathcal{H} = \mathcal{H}_0 + \boldsymbol{W} = \begin{pmatrix} E_1 & 0 \\ 0 & E_2 \end{pmatrix} + \begin{pmatrix} W_{11} & W_{12} \\ W_{21} & W_{22} \end{pmatrix}. \tag{33}$$

The eigenvectors are real so $W_{12} = W_{21}$. The Hamiltonian can be written as a linear combination of Pauli matrices

$$\mathcal{H} = \left(\frac{E_1 + E_2}{2} + \frac{W_{11} + W_{22}}{2}\right)\mathbf{1} + \left(\frac{E_1 - E_2}{2} + \frac{W_{11} - W_{22}}{2}\right)\boldsymbol{\sigma}_3 + W_{12}\boldsymbol{\sigma}_1 \tag{34}$$

we define

$$\Delta_s = 2\sqrt{\left(\frac{E_1 - E_2}{2} + \frac{W_{11} - W_{22}}{2}\right)^2 + W_{12}^2} \tag{35}$$

$$\tan(\theta) = \frac{2W_{12}}{(W_{11} - W_{22}) + (E_1 - E_2)}. \tag{36}$$

The eigenenergies are

$$E_n = \left(\frac{E_1 + E_2}{2} + \frac{W_{11} + W_{22}}{2}\right) \pm \frac{\Delta_s}{2}. \tag{37}$$

The eigenstates are found by rotating a spin half around the y axis at an angle θ

$$|+\rangle \longrightarrow \begin{pmatrix} \cos(\theta/2) \\ \sin(\theta/2) \end{pmatrix} \tag{38}$$

$$|-\rangle \longrightarrow \begin{pmatrix} -\sin(\theta/2) \\ \cos(\theta/2) \end{pmatrix}. \tag{39}$$

Assuming that the unperturbed basis consists of distinct dot-like and wire-like states, it follows that we can use the following approximation:

$$\Theta^{(+)} = \theta \tag{40}$$

$$\Theta^{(-)} = \pi - \theta. \tag{41}$$

Using equations (28) and (32), this implies

$$\sqrt{q_{\rm D}^{(+)} q_{\rm D}^{(-)}} \approx \frac{b}{2}|\sin(\theta)| \tag{42}$$

$$|\varphi_{\rm D}^{(+)} - \varphi_{\rm D}^{(-)}| = \frac{2}{\sqrt{b}}\left[\frac{1}{4}g\right]^{1/2}\frac{1}{|\sin(\theta)|}. \tag{43}$$

We note that in the strong mixing region we have $\theta \approx \pi/2$.

In the next sections, we obtain explicit expressions for the 'splitting' and the 'mixing' using the above scheme. From the numerics (see, e.g., figure 7), we see that these are in fact very satisfactory approximations.

8. Far field analysis

The eigenstates of the ring in the $\boldsymbol{X}$ region of interest as defined in equation (26) can be found using first-order perturbation theory with respect to the wire–dot coupling. This is explained below. We have verified numerically that the approximation is remarkable unless we are very close to a degeneracy point. This defines our distinction between 'far'- and 'near'-field regions. In the latter case, in the next section we present a complementary treatment using degenerate perturbation theory.

The unperturbed Hamiltonian in the far-field analysis corresponds to $X_1 = X_2 = \infty$. Using the notation as defined in the previous section, we take $|2\rangle$ as the nth wire state and $|1\rangle$ as the closest dot state from above. Hence,

$$E_1 = \frac{1}{2\mathsf{m}}\left(\frac{\pi}{L_{\mathrm{D}}}(1 + [n/b]_{\mathrm{integer}})\right)^2 \tag{44}$$

$$E_2 = \frac{1}{2\mathsf{m}}\left(\frac{\pi}{L_{\mathrm{W}}}n\right)^2. \tag{45}$$

Using the formula

$$W_{ij} = -\frac{1}{4\mathsf{m}^2 X}[\partial\psi^{(i)}][\partial\psi^{(j)}] \tag{46}$$

we get

$$W_{11} = -\frac{v_{\mathrm{E}}^2}{2L_{\mathrm{D}}}\left[\frac{1}{X_1} + \frac{1}{X_2}\right] \tag{47}$$

$$W_{22} = -\frac{v_{\mathrm{E}}^2}{2L_{\mathrm{W}}}\left[\frac{1}{X_1} + \frac{1}{X_2}\right] \tag{48}$$

$$|W_{12}| = \frac{v_{\mathrm{E}}^2}{2\sqrt{L_{\mathrm{D}}L_{\mathrm{W}}}}\left|\frac{1}{X_1} \pm \frac{1}{X_2}\right| \tag{49}$$

where the $\pm$ sign in the expression for the dot–wire coupling depends on whether the dot and the wire states have the same parity or not.

In the case of a far-field pumping cycle we start (say) with very high barriers and then lower one of them, say X_1. If we neglect the dot–wire coupling W_{12}, the dot level would cross the wire level at a point $X_1 = X^{(n)}$ that can be determined from the equation $E_1 + W_{11} = E_2$. At the vicinity of the avoided crossing, we obtain

$$|W_{12}| = \frac{1}{2\pi}(bg^{(n)})^{1/2}\Delta \tag{50}$$

where

$$g^{(n)} = \left(\frac{1}{v_{\mathrm{E}}}X^{(n)}\right)^{-2}. \tag{51}$$

From the condition $|W_{12}| \ll \Delta$ we deduce equation (26) which defines our $\boldsymbol{X}$ region of interest. Furthermore, from the results of the previous section we obtain expressions for the splitting and for the mixing of the levels:

$$\Delta_s = bg^{(n)}\frac{1}{2L}||\boldsymbol{X} - \boldsymbol{X}^{(r)}|| \tag{52}$$

$$\sin(\theta) = \frac{2}{\sqrt{bg^{(n)}}}\frac{v_{\mathrm{E}}}{||\boldsymbol{X} - \boldsymbol{X}^{(r)}||}. \tag{53}$$

We use the following notation, which we regard as a measure for the distance of the pumping cycle from the nearby degeneracy:

$$||\boldsymbol{X} - \boldsymbol{X}^{(r)}|| = \sqrt{(X_1 - X^{(n)})^2 + \frac{4}{b}\left(\frac{v_{\mathrm{E}}}{\sqrt{g^{(n)}}}\right)^2}. \tag{54}$$

The significance of this notation will be further clarified in the next section where we extend the analysis into the near-field region.

9. Near-field analysis

The unperturbed Hamiltonian in the near-field analysis corresponds to $X_1 = X_2 = X^{(r)}$. We can find a rough approximation for $X^{(r)}$ using the analysis of the previous section, but in fact we can find the exact expression which is derived in the appendix, where we also define the obvious notation k_r and $g^{(r)}$. For later calculation, the following approximation is useful:

$$X^{(r)} \approx \frac{v_{\mathrm{E}}}{\sqrt{g^{(r)}}}. \tag{55}$$

The unperturbed basis consists of the dot-like definite parity state $|1\rangle$ and the wire-like definite parity state $|2\rangle$. We recall that for these states Θ attains its extremal values as remarked at the end of the appendix. The energies of the unperturbed states are

$$E_1 = E_2 = E_r = \frac{1}{2\mathsf{m}}k_r^2 \tag{56}$$

and the perturbation matrix is

$$W_{11} = bg^{(r)}\frac{1}{2L}(\delta X_1 + \delta X_2) \tag{57}$$

$$W_{22} = g^{(r)}\frac{1}{2L}(\delta X_1 + \delta X_2) \tag{58}$$

$$|W_{12}| = \sqrt{b}g^{(r)}\frac{1}{2L}|\delta X_1 - \delta X_2| \tag{59}$$

where

$$\delta X_1 = X_1 - X^{(r)} \tag{60}$$

$$\delta X_2 = X_2 - X^{(r)}. \tag{61}$$

Consequently, we can determine both the splitting and the mixing of the levels:

$$\Delta_s = bg^{(r)}\frac{1}{2L}||\boldsymbol{X} - \boldsymbol{X}^{(r)}|| \tag{62}$$

$$\sin(\theta) = \frac{2}{\sqrt{b}}\frac{|X_1 - X_2|}{||\boldsymbol{X} - \boldsymbol{X}^{(r)}||}. \tag{63}$$

In the above expression, we have extended the interpretation of the distance measure as follows:

$$||\boldsymbol{X} - \boldsymbol{X}^{(r)}|| = \sqrt{(X_1 + X_2 - 2X^{(r)})^2 + \frac{4}{b}|X_1 - X_2|^2}. \tag{64}$$

Now we realize that the far-field results of the previous section are formally a saturated version of the near field results with

$$|X_1 - X_2|_\infty = \frac{v_{\mathrm{E}}}{\sqrt{g^{(n)}}}. \tag{65}$$

10. The expressions for G

We are now ready to calculate G from equation (6). There are of course G^{31} and G^{32} but the expressions look alike so we concentrate, say, on the case $X = X_1$ and suppress the node indication subscript whenever possible. By definition $\mathcal{F} = -\partial\mathcal{H}/\partial X = \delta(\hat{x} - x_1)$. The current operator has been defined in equation (2), but we still have the freedom to set x_0 as we want. So, the natural choice for the sake of calculation is obviously $x = x_1$. We shall expand later on the results that would be obtained if the current were measured via a different section. The matrix elements of the operators involved are

$$\begin{aligned}\mathcal{F}_{nm} &= -\frac{2}{L}\sqrt{q_{\mathrm{D}}^{(n)} q_{\mathrm{D}}^{(m)}}\,\sin\left(\varphi_{\mathrm{D}}^{(n)}\right)\sin\left(\varphi_{\mathrm{D}}^{(m)}\right)\\ \mathcal{I}_{nm} &= \mathrm{i}\frac{e}{\mathsf{m}L}\sqrt{q_{\mathrm{D}}^{(n)} q_{\mathrm{D}}^{(m)}}\left[\frac{k_n + k_m}{2}\sin\left(\varphi_{\mathrm{D}}^{(m)} - \varphi_{\mathrm{D}}^{(n)}\right) + \frac{k_n - k_m}{2}\sin\left(\varphi_{\mathrm{D}}^{(m)} + \varphi_{\mathrm{D}}^{(n)}\right)\right].\end{aligned} \tag{66}$$

One should note that $\mathcal{F}_{nm}$ is real and symmetric with respect to $n \leftrightarrow m$ interchange, while $\mathcal{I}_{nm}$ is antisymmetric and purely imaginary as implied by time-reversal symmetry. Once we sum equation (6) over all the occupied levels, nm terms cancel with mn terms. Within the framework of the 'two-level approximation' the only remaining term involves the occupied level n and the next empty level $m = n + 1$

$$G^{31}(X_1, X_2) = 2\frac{\mathcal{F}_{mn}\,\mathrm{Im}[\mathcal{I}_{nm}]}{\Delta_s^2}. \tag{67}$$

We recall the following expressions:

$$\sqrt{q_{\mathrm{D}}^{(+)} q_{\mathrm{D}}^{(-)}} \approx \frac{b}{2}|\sin(\theta)| \tag{68}$$

$$\varphi_{\mathrm{D}}^{(+)} \approx \varphi_{\mathrm{D}}^{(-)} \approx \left[\frac{1}{4}g\right]^{1/2} \tag{69}$$

$$\left|\varphi_{\mathrm{D}}^{(+)} - \varphi_{\mathrm{D}}^{(-)}\right| \approx \frac{2}{\sqrt{b}}\left[\frac{1}{4}g\right]^{1/2}\frac{1}{|\sin(\theta)|}. \tag{70}$$

Upon substitution we realize that both in the near and in the far field we can neglect the second term in the expression for $\mathcal{I}_{nm}$. Consequently,

$$G^{31}(X_1, X_2) = -\frac{1}{4}(gb)^{3/2}\frac{ev_{\mathrm{E}}}{L^2}\frac{1}{\Delta_s^2}|\sin(\theta)| = -\frac{2ev_{\mathrm{E}}}{b\sqrt{g}}\frac{|X_1 - X_2|}{||\boldsymbol{X} - \boldsymbol{X}^{(r)}||^3}. \tag{71}$$

We observe that in the near field, where $||\boldsymbol{X} - \boldsymbol{X}^{(r)}||$ is essentially the Euclidean measure of distance, we get the field of a Dirac monopole as expected. But as we go to the far field, the $|X_1 - X_2|$ contribution saturates as explained in the previous section.

11. The calculation of Q

Having found G^{31} and a similar expression for G^{32} we can perform the integration of equation (4) in order to obtain Q. We already pointed out that most of the contribution in the regions of our interest comes from the avoided crossings. In the near field it is most convenient to make the integration along $X_1 - X_2 = \pm\mathrm{const}$ segments, while in the case of the far field we make the integration along $X_2 = \infty$ and $X_1 = \infty$ segments.

It is not difficult to realize that in the near-field calculation both segments ($X_1 - X_2 = \pm\mathrm{const}$) give the same contribution. This means that we simply have to do one of the integrals

and to multiply by 2. But in the far field one should be more careful. If we measure the current in the *middle* of the dot (as indeed done in the numerics) then the same rule applies. But if we measure the current (say) at node 1, then the predominant contribution to Q comes obviously from the $X_2 = \infty$ segment, so the result should not be multiplied by 2. Performing a straightforward calculation of the $\mathrm{d}X$ integral, using

$$\int_{-\infty}^{+\infty} \frac{\mathrm{d}x}{(x^2 + a^2)^{3/2}} = \frac{2}{a^2} \tag{72}$$

and taking the above discussion into account, we get in the near field

$$Q \approx \frac{X^{(r)}}{|X_1 - X_2|} e. \tag{73}$$

One can show that this result is in agreement with the rough estimate of equation (14). However, in the far field we have to substitute the saturated value of $|X_1 - X_2|$ leading to the result $Q \approx e$.

The calculation in the far field does not care whether the pumping cycle encircle a $\Phi = 0$ degeneracy or a $\Phi = \pi$ degeneracy. It is only in the near field of $X^{(r)}$ that we see the difference. This is clearly confirmed by the numerics (figure 4). But a closer look reveals that the far-field numerical result for Q is somewhat smaller than 1. This might look like a contradiction with respect to the general expectations. The resolution of this puzzle is related to the limitation of the far-field perturbative treatment. Within the framework of this treatment $\Theta^{(n)}$ changes from $\Theta^{(n)} = \pi$ to $\Theta^{(n)} = 0$ as we lower (say) the X_1 barrier. But in fact we know from section 8 that Θ is bounded. This means that not all the probability gets into the dot region. Consequently, if we integrate along the $X_2 = \infty$ segment, we expect to get $Q < e$ as observed. On the other hand, in the case of a full pumping cycle, we have to cross from the $X_2 = \infty$ segment to the $X_1 = \infty$ segment. This was neglected in our calculation. Thus, if we had a full cycle we would expect to get $Q \approx e$ in the far field as implied by the Dirac chains picture.

12. Discussion

We were able to derive an estimate for Q in the case where the pumping cycle is dominated by a single degeneracy. Within this framework, we can still distinguish between near-field (where $Q \gg e$) and far-field (where $Q \sim e$) regions. Our results are in agreement with those of [3]. We note that an optional derivation of the near-field limit has been introduced in [10] using an extension of the BPT scattering formalism. But the latter derivation was not suitable to reproduce the far-field result because it has been *assumed* there that the charge cannot accumulate in the dot region.

It should be re-emphasized that the results that we have obtained assume that the pumping cycle is dominated by a single degeneracy. In a follow-up work [15], we shall discuss the case where the charge transport involves many levels, such that the contribution of neighbouring levels (in equation (6)) is negligible compared with the contribution that comes from $|m - n| > 1$ levels.

The results that we obtain for a closed geometry are very different from those that are obtained for an open geometry. This is because the motion of the electron is 'recycled'. In a more technical language this means that multiple rounds should be taken into account in the calculation of correlation functions. Reference [16, 4] further discuss how the Kubo formula can be used in order to interpolate these two extreme circumstances.

It should be clear that adiabatic transport becomes counter-intuitive if one adopts a misleading zero-order point of view of the adiabatic process. Moreover, even within the 'two-level approximation' it would not be correct to say that Q is determined by *peristaltic*

mechanism: namely, it is not correct to say that charge transfer is regulated by the Landau–Zener transitions.

A *peristaltic* mechanism would imply $Q \sim e$. In the near field, we have $Q \gg e$ so we do not have such mechanism for sure. This is also reflected by having the same I at both nodes as discussed in the paragraph of equation (73). However, even in the far field, where the peristaltic picture seems natural, we have realized that it is an over-simplification: also in the case of a far-field cycle a finite fraction of Q is contributed during the intermediate stages of the pumping cycle.

Acknowledgments

D C thanks M Moskalets and M Büttiker for discussions that had motivated this work, and Y Oreg for urging clarification of the formal result. We are grateful to T Kottos, H Schanz and G Rosenberg for helpful suggestions and help with the numerical procedure. The research was supported by the Israel Science Foundation (grant no. 11/02) and by a grant from the GIF, the German–Israeli Foundation for Scientific Research and Development.

Appendix. Finding the degeneracy points

If system is symmetric ($X_1 = X_2 = X$) then we can distinguish between odd and even states leading to the following eigenvalue equations:

$$\cot(kL_{\mathrm{D}}/2) + \cot(kL_{\mathrm{W}}/2) = -\frac{2\mathsf{m}}{k}X \qquad \text{odd states} \tag{A.1}$$

$$\tan(kL_{\mathrm{D}}/2) + \tan(kL_{\mathrm{W}}/2) = +\frac{2\mathsf{m}}{k}X \qquad \text{even states.} \tag{A.2}$$

As we lower X we have an exact crossing whenever a dot state crosses a wire state with the opposite parity. We have an avoided crossing whenever a dot state tries to cross a wire state with the same parity. The latter becomes an exact crossing if the flux through the ring is half-integer.

We can determine the degeneracy points by equating (A.1) with (A.2). This gives $\sin(kL_{\mathrm{W}}) = -\sin(kL_{\mathrm{D}})$. For half-integer flux it is convenient to use delta gauge on the middle of the wire, so as to get there π phase jump boundary conditions. This implies that in the above equation we make the replacement $(kL/2) \mapsto (kL/2) + (\pi/2)$, hence getting the degeneracy condition $\sin(kL_{\mathrm{W}}) = +\sin(kL_{\mathrm{D}})$. We therefore conclude that we have degeneracies for

$$k_r = \frac{\pi}{L_{\mathrm{W}} - L_{\mathrm{D}}} n_r. \tag{A.3}$$

They are categorized into $\Phi = 0$ degeneracies for $n_r = 1, 3, 5, \ldots$ and $\Phi = \pi$ degeneracies for $n_r = 2, 4, 6, \ldots$. Their location is $(X^{(r)}, X^{(r)})$ where

$$X^{(r)} = -\frac{k_r}{\mathsf{m}} \cot(k_r L_{\mathrm{D}}). \tag{A.4}$$

Accordingly,

$$g^{(r)} = g(X^{(r)}) = \sin^2(k_r L_{\mathrm{D}}) = \sin^2(k_r L_{\mathrm{W}}). \tag{A.5}$$

At a degeneracy point, the mixing parameter Θ that characterizes the odd and the even states attains the extremal values which are allowed by equation (27). This can be verified by deducing $q_{\mathrm{W}}/q_{\mathrm{D}}$ from equation (22) with $\varphi_{\mathrm{D}} = k_r L_{\mathrm{D}}/2$ for the odd state and $\varphi_{\mathrm{D}} = (\pi/2) + k_r L_{\mathrm{D}}/2$ for the even state.

References

[1] Kouwenhoven L P, Marcus C M, Mceuen P L, Tarucha S, Westervelt R M and Wingreen N S 1997 *Proc. Advanced Study Inst. on Mesoscopic Electron Transport* ed L L Sohn, L P Kouwenhoven and G Schon (Dordrecht: Kluwer)

[2] Cohen D 2002 *Preprint* cond-mat/0208233
Cohen D 2005 *Solid State Commun.* **133** 583

[3] Cohen D 2003 *Phys. Rev.* B **68** 155303

[4] For a mini-review see Cohen D 2005 *Physica* E **28** 308

[5] Rosenberg G and Cohen D 2006 *J. Phys. A: Math. Gen.* **39** 2287

[6] Levinson Y, Entin-Wohlman O and Wolfle P 2000 *Preprint* cond-mat/0010494

[7] Buttiker M, Thomas H and Pretre A 1994 *Z. Phys. B: Condens. Matter* **94** 133

[8] Brouwer P W 1998 *Phys. Rev.* B **58** R10135

[9] Shutenko T A, Aleiner I L and Altshuler B L 2000 *Phys. Rev.* B **61** 10366

[10] Moskalets M and Büttiker M 2003 *Phys. Rev.* B **68** 161311

[11] Berry M V 1984 *Proc. R. Soc.* A **392** 45

[12] Thouless D J 1983 *Phys. Rev.* B **27** 6083

[13] Avron J E, Raveh A and Zur B 1988 *Rev. Mod. Phys.* **60** 873

[14] Berry M V and Robbins J M 1993 *Proc. R. Soc.* A **442** 659

[15] Sela I and Cohen D (in preparation)

[16] Cohen D 2003 *Phys. Rev.* B **68** 201303